# The insulin-like growth factor pathway is altered in spinocerebellar ataxia type 1 and type 7

Jennifer R. Gatchel*, Kei Watase†, Christina Thaller‡, James P. Carson‡§, Paymaan Jafar-Nejad¶, Chad Shaw¶, Tao Zu‖, Harry T. Orr‖, and Huda Y. Zoghbi*,**††

Departments of *Neuroscience, ‡Biochemistry and Molecular Biology, and ¶Molecular and Human Genetics and **Howard Hughes Medical Institute, Baylor College of Medicine, Houston, TX 77030; †Tokyo Medical and Dental University, Tokyo 113-8519, Japan; §Pacific Northwest National Laboratory, Richland, WA 99354; and ‖Institute of Human Genetics, University of Minnesota, Minneapolis, MN 55455

Contributed by Huda Y. Zoghbi, November 30, 2007 (sent for review October 3, 2007)

**Polyglutamine diseases are inherited neurodegenerative disorders caused by expansion of CAG repeats encoding a glutamine tract in the disease-causing proteins. There are nine disorders, each having distinct features but also clinical and pathological similarities. In particular, spinocerebellar ataxia type 1 and 7 (SCA1 and SCA7) patients manifest cerebellar ataxia with degeneration of Purkinje cells. To determine whether the disorders share molecular pathogenic events, we studied two mouse models of SCA1 and SCA7 that express the glutamine-expanded protein from the respective endogenous loci. We found common transcriptional changes, with down-regulation of insulin-like growth factor binding protein 5 (*Igfbp5*) representing one of the most robust changes. *Igfbp5* down-regulation occurred in granule neurons through a non-cell-autonomous mechanism and was concomitant with activation of the insulin-like growth factor (IGF) pathway and the type I IGF receptor on Purkinje cells. These data define one common pathogenic response in SCA1 and SCA7 and reveal the importance of intercellular mechanisms in their pathogenesis.**

cerebellum | neurodegeneration | polyglutamine | Purkinje cell | granule neuron

Polyglutamine diseases are a group of inherited neurodegenerative disorders that include spinocerebellar ataxia (SCA) types 1, 2, 3, 6, 7, and 17 as well as Huntington disease (HD), dentatorubral–pallidoluysian atrophy (DRPLA), and spinal bulbar muscular atrophy (SBMA). They are caused by expansion of CAG repeats encoding a polyglutamine tract in different proteins (1). Evidence suggests that the polyglutamine expansion confers toxicity predominantly through a gain-of-function mechanism, although loss of function may also play a role (1, 2). Despite widespread expression of the disease proteins in the central nervous system (CNS), there is selective vulnerability of specific neurons in each disease (1). Such selective neuronal vulnerability gives rise to the specific features of each disease.

SCA1 and SCA7 have distinct features while also sharing some key similarities. In SCA1, primary symptoms include ataxia, dysarthria, and bulbar dysfunction, whereas cognitive impairment is more varied (1). This presentation is associated with cerebellar atrophy and loss of Purkinje cells (PCs) and secondary loss of granule neurons (1). In SCA7, progressive visual loss, cerebellar ataxia, and dysarthria are the most common clinical features (3). In addition to retinal degeneration, cerebellar PCs and neurons of the dentate nucleus and inferior olive are among the earliest to degenerate (3).

Given that SCA1 and SCA7 share a cerebellar degenerative phenotype, we proposed that some shared molecular changes might occur in both diseases, and that common molecular alterations could pinpoint pathways that could be targeted to modulate or monitor the pathogenesis of more than one disease. We focused on transcriptional changes because both ATXN1 and ATXN7 play roles in transcriptional regulation (4–8), and transcriptional defects can be detected in early-symptomatic stages of both SCA1 and SCA7 mouse models (9, 10).

To test our hypothesis, we examined cerebellar gene expression patterns in SCA1 and SCA7 knockin (KI) models—$Sca1^{154Q/2Q}$ mice and $Sca7^{266/5Q}$ mice. These mice express glutamine-expanded ATXN1 and ATXN7, respectively, in the endogenous pattern, and they accurately replicate disease features (10, 11). Here, we describe the identification of a signal transduction pathway—the insulin-like growth factor (IGF) pathway—that is affected in both diseases. The alterations we describe provide insight into cerebellar pathogenesis in SCA1 and SCA7 and might prove helpful in monitoring disease progression.

## Results

***Sca1*$^{154Q/2Q}$ and *Sca7*$^{266Q/5Q}$ Mice Share Cerebellar Gene Expression Changes.** We surveyed global transcriptional changes in $Sca1^{154Q/2Q}$ and $Sca7^{266Q/5Q}$ cerebellum using microarray technology. To capture early changes, we carried out experiments at an early symptomatic disease stage ($Sca1^{154Q/2Q}$ mice: 4, 9, and 12 weeks; $Sca7^{266Q/5Q}$ mice: 5 wks) (10, 11). [The timing of microarray and all subsequent experiments in the context of $Sca1^{154Q/2Q}$ and $Sca7^{266Q/5Q}$ disease progression is provided in supporting information (SI) Fig. 7 *a* and *b*.]

We found significant concordance between $Sca1^{154Q/2Q}$ and $Sca7^{266Q/5Q}$ cerebellar expression patterns ($P = 0.00040$), with 31 probe sets commonly misregulated (SI Tables 1 and 2). Of note is that 26 of the 31 differentially regulated probe sets in both $Sca1^{154Q/2Q}$ and $Sca7^{266Q/5Q}$ cerebellum were down-regulated in both models, whereas only 5 were up-regulated (SI Table 2). This predominance of down-regulation is itself significant ($P = 0.00019$).

Ontology analysis revealed that genes involved in growth factor-binding protein complexes and inositol kinase and phosphatase activities were among those enriched in this overlap list (SI Figs. 8–13). Despite the significant overlap between $Sca1^{154Q/2Q}$ and $Sca7^{266Q/5Q}$ datasets, many differentially expressed genes were specific to each model [NCBI Gene Expression Omnibus (GEO) accession no. GSE9914]. These included genes involved in mRNA processing and chromatin ($Sca1^{154Q/2Q}$) and those involving transcription factor-binding and MHC class I proteins ($Sca7^{266Q/5Q}$) (SI Figs. 14–19).

Author contributions: J.R.G., K.W., H.T.O., and H.Y.Z. designed research; J.R.G., K.W., C.T., P.J.-N., and T.Z. performed research; J.P.C. contributed new reagents/analytic tools; J.R.G., C.S., and T.Z. analyzed data; and J.R.G. and H.Y.Z. wrote the paper.

The authors declare no conflict of interest.

Freely available online through the PNAS open access option.

Data deposition: The data reported in this paper have been deposited in the Gene Expression Omnibus (GEO) database, www.ncbi.nlm.nih.gov/geo (accession no. GSE9914).

††To whom correspondence should be addressed. E-mail: hzoghbi@bcm.tmc.edu.

This article contains supporting information online at www.pnas.org/cgi/content/full/0711257105/DC1.

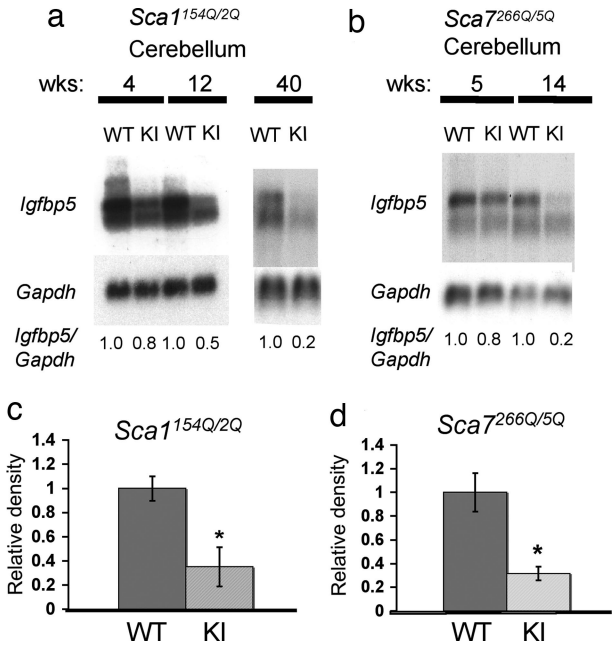


**Fig. 1.** *Igfbp5* RNA is decreased in *Sca1*$^{154Q/2Q}$ and *Sca7*$^{266Q/5Q}$ cerebellum. (*a* and *b*) Northern blots of cerebellar RNA at early-symptomatic (*Sca1*$^{154Q/2Q}$, 4 and 12 weeks; *Sca7*$^{266Q/5Q}$, 5 weeks) and late-symptomatic (*Sca1*$^{154Q/2Q}$, 40 weeks; *Sca7*$^{266Q/5Q}$, 14 weeks) disease stages show progressive down-regulation of *Igfbp5* RNA. (*c* and *d*) Quantification of *Igfbp5* RNA relative to *Gapdh* using multiple animal pairs ($n = 3$ pairs of *Sca1*$^{154Q/2Q}$ and WT controls; $n = 5$ and 4 of *Sca7*$^{266Q/5Q}$ and WT mice, respectively) shows significant down-regulation of *Igfbp5* in late-symptomatic cerebellum. Values represent mean ± SEM. The asterisks indicate significant genotype differences (*, $P < 0.05$).

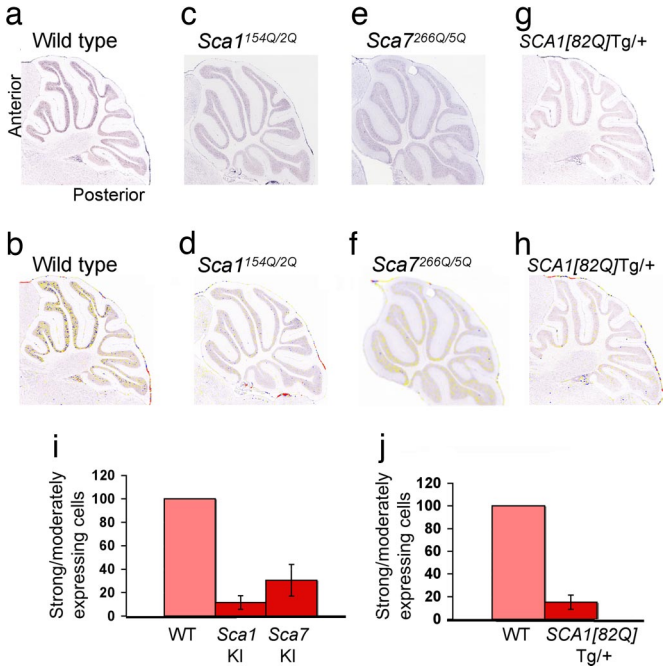


**Fig. 2.** *Igfbp5* is decreased in the cerebellar granule layer of *Sca1* and *Sca7* KI mice and in *SCA1[82Q]* PC-specific Tg mice. (*a–h*) Representative ISH images for *Igfbp5* (*a*, *c*, *e*, and *g*) and pseudocolored sagittal sections (*b*, *d*, *f*, and *h*) with *Igfbp5*-expressing cells colored according to their expression level (red, strong; blue, moderate; yellow, weak). (*i*) Quantification of strongly and moderately expressing cells reveals a decrease in *Sca1*$^{154Q/2Q}$ (18–19 weeks) and *Sca7*$^{266Q/5Q}$ (12–13 weeks) cerebellum compared with WT. A decrease is also observed when mutant ATXN1 is only expressed in PC, in *SCA1[82Q]*Tg/+ (22–23 weeks) cerebellum. $n = 2$ KI and 2 WT animals for both *Sca1*$^{154Q/2Q}$ and *Sca7*$^{266Q/5Q}$ and 2 Tg/+ and 2 WT littermates for *SCA1[82Q]*, with 40–47 sections quantified per animal. KI and Tg/+ expression values are shown as a percentage of WT. Values represent mean ± SEM.

***Igfbp5* Is Down-Regulated in *Sca1*$^{154Q/2Q}$ and *Sca7*$^{266Q/5Q}$ Cerebellum.** The most significant common gene expression change based on fold change was the down-regulation of *Igfbp5* (SI Table 1), a key component of the IGF axis (12). Northern blot analysis confirmed the down-regulation of *Igfbp5* at an early disease stage in both *Sca1*$^{154Q/2Q}$ and *Sca7* $^{266Q/5Q}$ cerebellum (Fig. 1 *a* and *b*). Furthermore, this down-regulation was progressive, such that RNA levels at the late disease stage (40 weeks in *Sca1* KI and 14 weeks in *Sca7* KI) were <60% of those of WT animals (Fig. 1 *c* and *d*). These changes were specific to vulnerable brain regions, because we did not find similar changes in cortex, a tissue relatively unaffected in pathogenesis (SI Fig. 20).

***Igfbp5* Is Down-Regulated in a Non-Cell-Autonomous Manner in the Granule Layer of the Cerebellar Cortex.** Because *Igfbp5* changed progressively in both *Sca1*$^{154Q/2Q}$ and *Sca7*$^{266Q/5Q}$ cerebellum, we were interested in determining the cell types in which the expression changes were occurring. Because PCs are among the most severely affected neurons in SCA1 and SCA7, we hypothesized that *Igfbp5* might be expressed and down-regulated in these neurons. To test this hypothesis, we performed *in situ* hybridization (ISH) experiments and found that within the cerebellum, *Igfbp5* was predominantly expressed in the granule layer (Fig. 2 and SI Fig. 21*b*). The size, number, and location of the cells in which this intense signal was found were all consistent with granule neurons. Expression was also found in the deep cerebellar nuclei, whereas signal in other layers of the cerebellar cortex was extremely sparse. In addition, we found a sharp anterior–posterior gradient of *Igfbp5* expression in the cerebellar cortex. Expression was highest in the anterior compartment (lobules I–VI) and was marked by a boundary in lobule VI (Fig. 2 *a* and *b*). Importantly, this expression pattern was observed independently by using a different probe and methodology (13).

We used custom-designed imaging software (14) to pseudocolor and quantify *Igfbp5* expressing cells from tissue sections spanning entire cerebellar hemispheres (Fig. 2 *b*, *d*, and *f*). This analysis confirmed that the highest level of *Igfbp5* occurred in the anterior granule compartment (Fig. 2*b*). Expression was dramatically decreased in *Sca1*$^{154Q/2Q}$ and *Sca7*$^{266Q/5Q}$ cerebellum (Fig. 2 *c–f* and *i*). Expression of *Fgf-1*, an anterior granule compartment marker (15), and *Igfbpl1*, an additional growth factor pathway component, were not altered (SI Fig. 21 *c–f*), indicating that the decrease in *Igfbp5* was specific and not due to a general expression deficiency of all anterior compartment genes or growth factors.

To gain insight into the nature of *Igfbp5* down-regulation in granule neurons and determine whether it was or was not cell autonomous, we used an SCA1 transgenic (Tg) mouse model (*SCA1[82Q]*Tg) that expresses a mutant *SCA1* allele encoding ATXN1 with 82 glutamines only in PCs (16) and develops a progressive cerebellar degenerative phenotype (SI Fig. 7*c*). ISH experiments and quantification revealed a decrease in *Igfbp5* expression in the cerebella of these mice (Fig. 2 *g*, *h*, and j). This suggested that the down-regulation of *Igfbp5* in the cerebellar granule layer occurred by a non-cell autonomous mechanism, because it occurred when the mutant protein was expressed only in PCs.

***Igfbp5* Down-Regulation Is Coupled with Increased Activation of the IGF1R.** To probe the underlying cause of *Igfbp5* down-regulation, we examined other IGF axis components. Given the role of

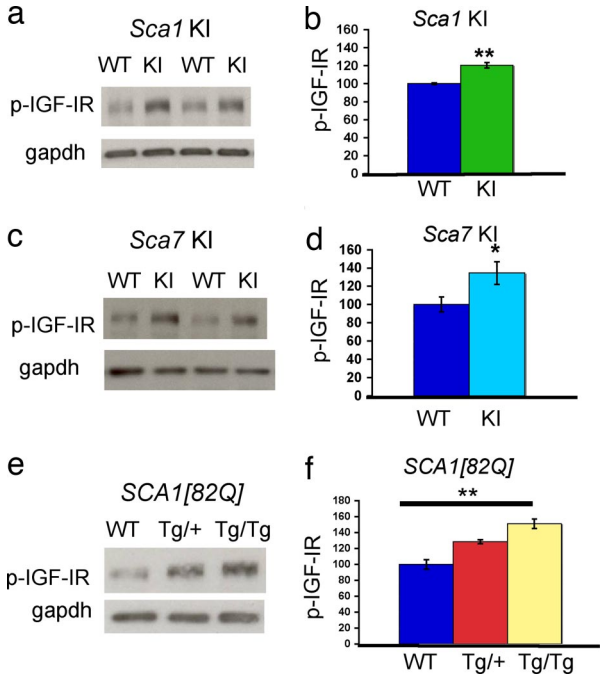


**Fig. 3.** IGF1R phosphorylation is increased in *Sca1*$^{154Q/2Q}$, *Sca7*$^{266Q/5Q}$, and *SCA1[82Q]* Tg cerebellum. (*a*, *c*, and *e*) Western blot analyses using cerebellar protein extracts from *Sca1*$^{154Q/2Q}$ (49–52 weeks) and *Sca7*$^{266Q/5Q}$ (12–13 weeks) mice and *SCA1[82Q]* (8–10 weeks) mice and antibodies to the phosphorylated (active) form of the IGF1R as well as to Gapdh. (*b*, *d*, and *f*) Quantification of phospho-IGF1R levels relative to Gapdh using multiple pairs of KI, Tg, and WT animals ($n = 3$; see *Methods*) indicates a significant increase in *Sca1* KI and *Sca7* KI vs. WT (*b* and *d*) as well as a significant increase in *SCA1[82Q]*Tg/Tg and Tg/+ compared with WT (*f*). Values represent mean ± SEM. The asterisks indicate significant genotype differences (*, $P < 0.05$; **, $P < 0.01$).

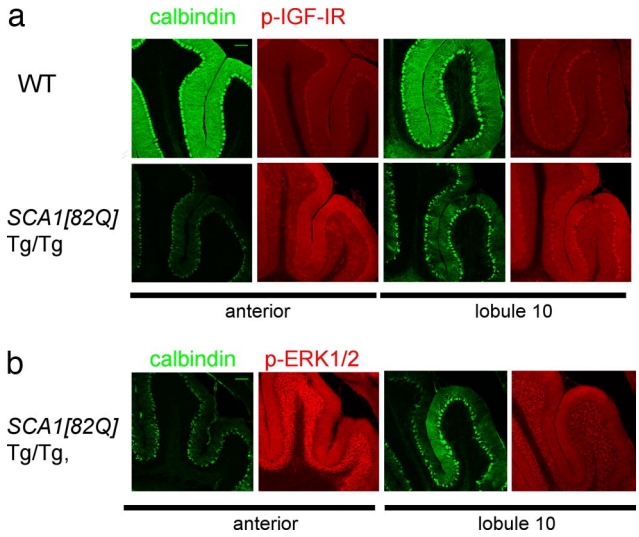


**Fig. 4.** Patterns of IGF1R and ERK1/2 phosphorylation relative to PC pathology in *SCA1[82Q]*Tg/Tg cerebellum. (*a*) Representative confocal images from 11-week-old *SCA1[82Q]*Tg/Tg and WT mice showing calbindin and phospho-IGF1R immunostaining in sections from anterior cerebellar lobules and from lobule 10. (*b*) Calbindin immunostaining is decreased, and phospho-IGF1R levels are increased in the PC, molecular, and granule layers in Tg/Tg cerebellum compared with WT. Immunoreactivity for phosphorylated ERK, which is increased in *SCA1[82Q]*Tg/Tg cerebellum (SI Fig. 24*a*), occurs most prominently in anterior lobules compared with lobule 10. Similar results were obtained from three pairs of *SCA1[82Q]*Tg/Tg and WT mice (three to four sections per animal) in four independent experiments. (Scale bars, 100 μm.)

Igfbp5 in influencing IGF1 bioavailability (12), we determined whether the biological effects of IGF1, which are mainly mediated through the IGF1R, were altered. On binding to IGF1, the cytoplasmic portion of the IGF1R is phosphorylated, creating a binding site for IRS-1 and phosphatidyl-inositol-3-kinase (PI3-K). These substrates subsequently play a role in IGF1R-mediated protection and proliferation by recruiting downstream phosphorylation events, including activation of Akt and Ras/MAPK (17).

Given the potential of Igfbp5 to block the availability of IGF1 for its receptor (18, 19), we hypothesized that in *Sca1* and *Sca7* KI cerebellum, decreased *Igfbp5* expression would lead to an increased amount of IGF1 available to activate the IGF1R and downstream signaling. To test this hypothesis, we examined IGF1R phosphorylation in cerebellar homogenates from *Sca1* and *Sca7* KI mice. We found a significant increase in IGF1R phosphorylation in KI cerebellum (Fig. 3 *a–d*). To determine whether expression of mutant polyglutamine protein exclusively in PCs was sufficient to confer this increase, we collected homogenates from WT, *SCA1[82Q]*Tg/+, and *SCA1[82Q]*Tg/Tg, mice. We again found a significant increase in IGF1R activation (Fig. 3 *e* and *f*). Thus, the significant decrease in *Igfbp5* expression was accompanied by an increase in IGF1R activation.

For further IGF pathway studies, we focused on SCA1 pathology, given the availability of knockin, PC-specific, and conditional models of disease (11, 16, 20). Within the cerebellar cortex, the IGF1R is expressed on PC soma and dendrites, in presynaptic axon terminals in the molecular layer, and in mossy-fiber rosettes and granule-cell soma; expression in glia and in endothelial cells has also been observed (21). We carried out immunostaining experiments and found increased receptor phosphorylation in these populations in *SCA1[82Q]*Tg/Tg cerebellum compared with WT, particularly in the PC and molecular layers, as well as intense staining in the granule layer (Fig. 4*a*). A similar pattern was observed in *Sca1*$^{154Q/2Q}$ cerebellar cortex (SI Fig. 22).

The increased IGF1R activation occurred in conjunction with increased activation of the downstream effectors, phosphorylated-Akt and -Erk, in *SCA1[82Q]*Tg/Tg cerebellum (SI Figs. 23 and 24*a*). Interestingly, relatively less granule layer phospho-IGF1R immunoreactivity and phospho-ERK activation was found in lobule 10 of *SCA1[82Q]* cerebellum compared with anterior lobules (Fig. 4 *a* and *b* and SI Fig. 24*a*); lobule 10 was also relatively spared in disease compared with anterior lobules based on coimmunofluorescence with calbindin, a protein that labels PC dendrites (Fig. 4 and SI Fig. 24). This suggested that activation in certain cell types occurred most prominently in regions of enhanced neuronal vulnerability.

**The Down-Regulation of *Igfbp5* Is Reversible Upon Modulation of Mutant ATXN1 Expression.** The pathology induced by polyglutamine-expanded proteins can be partially reversed if mutant protein expression is halted early enough in disease (22). Specifically, in a conditional *SCA1* mouse model, the PC specific expression of mutant ATXN1 with 82 glutamines can be turned off with the administration of doxycyline, resulting in rescue of both clinical features and cellular pathology (20).

To determine whether *Igfbp5* down-regulation was responsive to the disease state, we collected cerebellar RNAs from WT animals and from four groups of conditional Pcp2-tTA(Tg/+)/TRE-*SCA1[82Q]*(Tg/Tg) littermate animals: age-matched 12-week-old mice in which the *SCA1* transgene had never been turned off and mice in which the *SCA1* transgene had been expressed for 12 weeks and then turned off for either 4, 8, or 12 weeks. Reduction of mutant ATXN1 expression resulted in a gradual, significant increase in *Igfbp5* levels to near WT (Fig. 5).

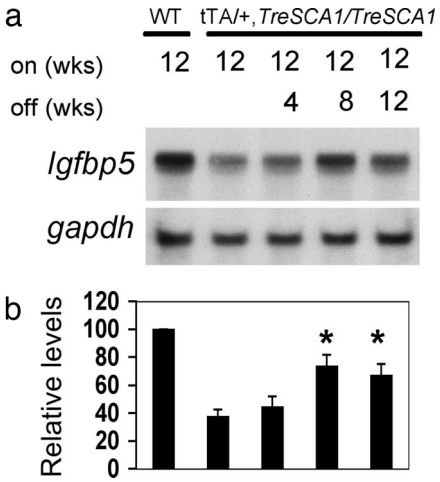


**Fig. 5.** *Igfbp5* down-regulation is reversible in an *SCA1[82Q]* conditional mouse model. (*a*) Northern blot analysis shows the gradual recovery of *Igfbp5* RNA levels after the mutant SCA1 transgene has been turned off for 4, 8, or 12 weeks. (*b*) *Igfbp5* RNA levels relative to *Gapdh* in *SCA1[82Q]* cerebellum were normalized to WT, with three animals in each group. Data are expressed as mean ± SEM; (*, $P < 0.05$).

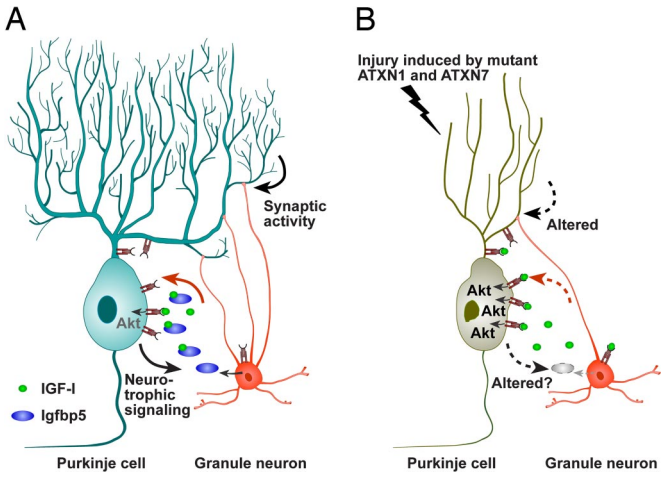


**Fig. 6.** Model of Igfbp5 and IGF1 signaling in normal (*A*) and in $Sca1^{154Q/2Q}$, $Sca7^{266Q/5Q}$, and *SCA1[82Q]* (*B*) cerebellum. *Igfbp5* is expressed in granule neurons, whereas the IGF1R is more broadly expressed, suggesting possible cross-talk between PCs and granule neurons. In normal cerebellum, IGF1 can be bound by Igfbp5, which influences its availability for the IGF1R (*A*). Mutant ATXN1- and ATXN7-induced PC injury causes down-regulation of *Igfbp5* in granule neurons by a non-cell-autonomous mechanism (*B*). This mechanism may involve IGF1, expressed in part by PCs or, alternatively, could result from granule neurons sensing altered synaptic activity at granule–PC–parallel fiber connections. Given the increased IGF1R activation in $Sca1^{154Q/2Q}$, $Sca7^{266Q/5Q}$, and *SCA1[82Q]* cerebellum, we propose a model in which down-regulation of *Igfbp5* in granule neurons influences the local actions of IGF1, in part by increasing the availability of IGF1 for its receptor on PCs, which can lead to activation of downstream effectors such as Akt.

Thus, the changes in *Igfbp5* closely correlate with the disease state in SCA1.

## Discussion

**Common Transcriptional Changes Occur in Early-Symptomatic $Sca1^{154Q/2Q}$ and $Sca7^{266Q/5Q}$ Cerebellum.** The overlapping cerebellar phenotypes in SCA1 and SCA7 raised the possibility that these two disorders share some molecular pathogenic changes. Through analysis of $Sca1^{154Q/2Q}$ and $Sca7^{266Q/5Q}$ mice, we show that there are shared transcriptional changes that happen early in disease and, at least for *Igfbp5*, are specific to pathogenesis.

ATXN1 and ATXN7 each affect transcription in a context-specific fashion (4–8), and many of the categories of gene changes in our microarray studies were $Sca1^{154Q/2Q}$- or $Sca7^{266Q/5Q}$-specific (SI Figs. 14–19). This indicates that distinct processes are likely central to the pathogenesis of each disorder, which may partly reflect the role ATXN1 in RNA binding and ATXN7 in a histone acetyltransferase (HAT) complex (7, 8, 23). In contrast, many of the common gene changes, including *Igfbp5*, are not likely direct targets of ATXN1- and ATXN7-mediated pathogenesis, but, rather, represent shared early events in a cerebellar response. *Igfbp5* down-regulation may further be part of a more general response to neuronal injury. We describe this down-regulation at early disease stages in response to ATXN1- and ATXN7-induced injury, but changes in *Igfbp5* levels have also been reported at symptomatic/late-symptomatic disease stages in models based on overexpression of mutant polyglutamine proteins (24). It would be interesting to determine whether these reported changes also occur at earlier disease stages as they might hint that several degenerative disorders share some pathogenic responses. Thus, we describe a common transcriptional read-out of the early disease state that could potentially be used to pinpoint ways to modulate and monitor pathogenesis in more than one disorder.

**Non-Cell-Autonomous Down-Regulation of *Igfbp5*: A Role for PC-Driven Neuron–Neuron Interactions in SCA1 and SCA7 Pathogenesis.** Despite the primary PC pathology in SCA1 and SCA7, expression and down-regulation of *Igfbp5* occurred in the cerebellar granular layer. Even more remarkably, we show that *Igfbp5* down-regulation takes place through a non-cell-autonomous mechanism. Previous work supporting the importance of intercellular interactions in polyglutamine disorders has relied on the use of a truncated fragment of huntingtin or the overexpression of the mutant ATXN7 protein in cells that provide support to PCs (25–27). To date, however, this issue has not been investigated in KI models, whereby the mutant protein is expressed in the endogenous manner such that intercellular interactions and their influence on selective vulnerability can be investigated in the endogenous disease context. In this study, we show that whether PC injury arises from endogenous or cell-specific expression of full-length mutant polyglutamine protein, a similar transcriptional change occurs in granule neurons, indicating that this change is driven at least in part from a pathogenic response initiated in affected PCs.

It is interesting to consider how PC injury might be conveyed to the granule neuron to cause the decrease in *Igfbp5*. Expression of mutant ATXN1 in SCA1 mouse models leads to reduction in PC dendritic arborization (11, 16). Thus, one possibility is that changes in PC dendrites—the postsynaptic targets of granule cell parallel fibers—result in altered PC-granule neuron synaptic contacts that could trigger gene expression changes in granule neurons. Another possibility is that mutant ATXN1 or ATXN7 induces decreased expression of IGF1 in PCs, which in turn could drive this change, given that IGF1 levels can influence *Igfbp5* expression (28, 29) (Fig. 6).

No matter what the mechanism, concomitant changes in granule neurons and in PCs implicate cell–cell interactions in the pathogenesis of these disorders in the cerebellum (Fig. 6). The findings from these two disease models thus underscore the role of *Igfbp5* and the IGF pathway as a means of PC–granule neuron communication, particularly under conditions of stress.

***Igfbp5* Down-Regulation Occurs in the Context of Additional IGF Pathway Misregulation.** The finding of additional IGF pathway misregulation provides insight into how *Igfbp5* down-regulation

might influence pathogenesis in SCA1 and SCA7 models. Igfbp5 can have a context-specific effect on IGF1 activity (30), including the potential to inhibit IGF1 action when present in excess in an *in vitro* cerebellar model (19). Furthermore, when cerebellar granule neurons *in vitro* undergo KCl deprivation, *Igfbp5* is down-regulated, whereas the IGF1R is transiently increased, which may reflect an attempt to maximize IGF1 signaling (31). The changes we observe in $Sca1^{154Q/2Q}$, $Sca7^{266Q/5Q}$, and *SCA1[82Q]* cerebellum may similarly represent an adaptive attempt to maximize such signaling in the face of mutant ATXN1 and ATXN7 stress.

IGF1 signaling can have neuroprotective effects in the context of specific mutant polyglutamine proteins (32, 33). Indeed, IGF1 is a pleiotropic neuroprotective factor that may prevent the tissue atrophy, vascular dysfunction, and accumulation of deleterious products often associated with the aging brain (34). As such, compensatory responses to maximize IGF1 signaling in $Sca1^{154Q/2Q}$ and $Sca7^{266Q/5Q}$ mice could serve a protective role.

However, prolonged activation of neurotrophic signaling may also be maladaptive in neurodegeneration (35). Indeed, attenuation of IGF1 downstream signaling results in lifespan extension in *Caenorhabditis elegans*, *Drosophila*, and mice (36), suggesting that the outcome of such signaling may be context- and dose-dependent. IGF pathway activation may become deleterious in the context of mutant ATXN1, given that phosphorylation of ATXN1 at Ser-776, a putative Akt site, promotes stabilization and accumulation of mutant ATXN1 and that PI3-K/Akt enhance neurodegeneration in a *Drosophila* SCA1 model (37, 38). It is of interest that we found relative preservation of PCs in cerebellar lobule 10 of *SCA1[82Q]* mice and less IGF1R activation and phospho-ERK activation in this lobule. Thus, although IGF pathway changes could be adaptive responses to pathology, our data suggest that chronic overstimulation of this pathway may adversely modulate pathogenesis in these disorders.

***Igfbp5* Expression Is Tightly Correlated with the Disease State.** The change in *Igfbp5* we describe occurs very early in two disease models of SCA1 and SCA7. This and the responsiveness of *Igfbp5* expression to the disease state are key properties of a biomarker and raise the possibility that *Igfbp5* or other pathway components could be used in this capacity in these or other disorders. In sum, the common changes we describe, in addition to providing insight into the role of intercellular signaling in the cerebellar cortex as part of the pathogenic response in SCA1 and SCA7, may provide future opportunities to modulate and monitor disease course in these devastating diseases.

## Materials and Methods

**Animals.** $Sca1^{154Q/2Q}$, $Sca7^{266Q/5Q}$, *SCA1[82Q]*, and *SCA1[82Q]* conditional Tg mice have been described (10, 11, 16, 20). Additional details are available in *SI Text*. Experiments were in accordance with protocols approved by the Institutional Animal Care and Use Committees (IACUC) of Baylor College of Medicine and the University of Minnesota.

**Microarray Studies and Other Statistical Analysis.** Cerebella were dissected on a chilled glass plate and total RNA isolated by using TRIzol (Invitrogen), followed by clean-up over RNeasy mini columns (Qiagen) according to manufacturers' protocols. For *Sca1* KI, $n = 3$ per genotype at both 4 weeks and at 9–12 weeks. For *Sca7* KI, $n = 5$ per genotype at 5 weeks. cDNA synthesis, *in vitro* transcription, and hybridization onto oligonucleotide arrays (Mouse Expression Array 430A (*Sca1* samples), or Mouse Genome 430 2.0 Array (*Sca7*) were carried out by the University of California (Los Angeles) or the Baylor College of Medicine Microarray Core Facilities, respectively. Details of data normalization and analysis are available in *SI Text*. An ANOVA and linear contrasts to estimate KI vs. WT differences were computed for *Sca1* and *Sca7* datasets. To determine the concordance between the *Sca1* and *Sca7* contrasts, a Spearman's rank correlation analysis of the contrast scores and a Kendall's $\tau$ analysis of the "up-regulated" vs. "down-regulated" genes lists for the *Sca1* and *Sca7* experiments were calculated. *T* tests at the $P < 0.01$ level identified 667 down- vs. 349 up-regulated probe sets (*Sca1*), and 157 down- vs. 196 up-regulated probe sets (*Sca7*) (NCBI GEO database, accession GSE9914). A binomial test of proportions against the null hypothesis of equal proportion was computed to analyze the asymmetric distribution of up- and down-regulated probe sets in the commonly misregulated list.

For Northern blot experiments, KI, Tg, and WT differences were evaluated by using independent sample *t* tests. Western blot data were analyzed by using an independent sample *t* test for KI vs. WT differences, or a one-way ANOVA for *SCA1[82Q]*Tg data.

**RNA Studies.** Total cerebellar or cortical RNA was extracted by using TRIzol (Invitrogen), and Northern blot was performed as described (20). *Igfbp5* RNA levels were normalized to the amount of *Gapdh* per lane. For ISH, brains from $Sca1^{154Q/2Q}$, $Sca7^{266Q/5Q}$, and *SCA1[82Q]*Tg/+ mice were frozen in optimal cutting temperature (OCT). ISH on brain sections using a robotic platform, and quantitative analysis of the ISH signal using the Celldetekt protocol were carried out as described in ref. 14 and www.genepaint.org/RNA.htm. Additional details and probe descriptions are available in *SI Text*. Details of animal age and numbers are in figure legends.

**Western Blotting.** Animals were killed by rapid cervical dislocation and cerebella dissected on a chilled glass plate and homogenized in 1× RIPA Buffer [150 mM NaCl, 0.1% SDS, 1% Triton X-100, 50 mM Tris·HCl (pH 7.6)] with inhibitors [Complete Protease Inhibitors (Roche); phosphatase inhibitor cocktails I and II (Sigma)]. Samples were sonicated for 1–2 seconds, followed by centrifugation. Supernatants were flash-frozen in liquid nitrogen and stored at −80°C.

Proteins were evaluated by Western blotting according to standard procedures (11). Details of antibody dilutions, immunoblotting, and quantification are provided in *SI Text*. Analysis results are shown for three *Sca1* KI and three WT littermates at 49–52 weeks; three *Sca7* KI and three WT littermates at 12–13 weeks; and three *SCA1[82Q]*Tg/Tg, three Tg/+ and three age-, sex-, and strain-matched WT mice at 8–10 weeks. Results were repeated with two additional cohorts, each consisting of two to three KI and three WT mice (for both *Sca1* and *Sca7* KI) and with one additional cohort of *SCA1[82Q]*Tg/Tg, Tg/+ and WT mice.

**Immunofluorescence.** Details of perfusion, fixation, and immunolabeling with mouse anti-calbindin antibody (1:1,000; Sigma) and image capture are available in *SI Text*. Experiments were carried out by using three *SCA1[82Q]*Tg/Tg, three Tg/+, and three age-, sex-, and strain-matched WT mice at 11 weeks and one additional cohort at 20 weeks.

**ACKNOWLEDGMENTS.** We thank Y. Sun and N. Ao for technical assistance; M. Yaylaoglou, Y. Liu, and A. Liang of the Baylor College of Medicine ISH core; the Baylor College of Medicine Microarray Core; Y. Klisch for artwork; and members of the H.Y.Z. laboratory for critical discussion. This work was supported by National Institutes of Health Grants NS27699 (to H.Y.Z.) and NS22920 (to H.T.O.), Department of Energy Laboratory Directed Research and Development Grant DE-AC05-76RL01830 (to J.P.C.), National Research Service Award Grant 1 F30 MH072117 (to J.R.G.), and Baylor College of Medicine, Mental Retardation Developmental Disabilities Research Center Gene Expression Core Grant HD024064.

1. Orr HT, Zoghbi HY (2007) Trinucleotide repeat disorders. *Annu Rev Neurosci* 30:575–621.
2. Borrell-Pages M, Zala D, Humbert S, Saudou F (2006) Huntington's disease: From huntingtin function and dysfunction to therapeutic strategies. *Cell Mol Life Sci* 63:2642–2660.
3. Stevanin G, *et al.* (1998) Spinocerebellar ataxia type 7. *Analysis of Triplet Repeat Disorders*, ed Hayden MR, Rubinsztein DC (BIOS Scientific, Oxford, UK), pp 155–168.
4. Tsai CC, *et al.* (2004) Ataxin 1, a SCA1 neurodegenerative disorder protein, is functionally linked to the silencing mediator of retinoid and thyroid hormone receptors. *Proc Natl Acad Sci USA* 101:4047–4052.
5. Serra HG, *et al.* (2006) RORalpha-mediated Purkinje cell development determines disease severity in adult SCA1 mice. *Cell* 127:697–708.
6. Lam YC, *et al.* (2006) ATAXIN-1 interacts with the repressor Capicua in its native complex to cause SCA1 neuropathology. *Cell* 127:1335–1347.
7. Helmlinger D, *et al.* (2006) Glutamine-expanded ataxin-7 alters TFTC/STAGA recruitment and chromatin structure leading to photoreceptor dysfunction. *PLoS Biol* 4:e67.
8. Palhan VB, *et al.* (2005) Polyglutamine-expanded ataxin-7 inhibits STAGA histone acetyltransferase activity to produce retinal degeneration. *Proc Natl Acad Sci USA* 102:8472–8477.
9. Serra HG, *et al.* (2004) Gene profiling links SCA1 pathophysiology to glutamate signaling in Purkinje cells of transgenic mice. *Hum Mol Genet* 13:2535–2543.
10. Yoo SY, *et al.* (2003) SCA7 knockin mice model human SCA7 and reveal gradual accumulation of mutant ataxin-7 in neurons and abnormalities in short-term plasticity. *Neuron* 37:383–401.

11. Watase K, *et al.* (2002) A long CAG repeat in the mouse Scal locus replicates SCA1 features and reveals the impact of protein solubility on selective neurodegeneration. *Neuron* 34:905–919.
12. Beattie J, Allan GJ, Lochrie JD, Flint DJ (2006) Insulin-like growth factor-binding protein-5 (IGFBP-5): A critical member of the IGF axis. *Biochem J* 395:1–19.
13. Lein ES, *et al.* (2007) Genome-wide atlas of gene expression in the adult mouse brain. *Nature* 445:168–176.
14. Carson JP, Eichele G, Chiu W (2005) A method for automated detection of gene expression required for the establishment of a digital transcriptome-wide gene expression atlas. *J Microsc* 217:275–281.
15. McAndrew PE, *et al.* (1998) Novel receptor protein tyrosine phosphatase (RPTPrho) and acidic fibroblast growth factor (FGF-1) transcripts delineate a rostrocaudal boundary in the granule cell layer of the murine cerebellar cortex. *J Comp Neurol* 391:444–455.
16. Burright EN, *et al.* (1995) SCA1 transgenic mice: a model for neurodegeneration caused by an expanded CAG trinucleotide repeat. *Cell* 82:937–948.
17. Kulik G, Klippel A, Weber MJ (1997) Antiapoptotic signalling by the insulin-like growth factor I receptor, phosphatidylinositol 3-kinase, and Akt. *Mol Cell Biol* 17:1595–1606.
18. Kalus W, *et al.* (1998) Structure of the IGF-binding domain of the insulin-like growth factor-binding protein-5 (IGFBP-5): Implications for IGF, IGF-I receptor interactions. *EMBO J* 17:6558–6572.
19. Zhong J, Deng J, Ghetti B, Lee WH (2002) Inhibition of insulin-like growth factor I activity contributes to the premature apoptosis of cerebellar granule neuron in weaver mutant mice: *in vitro* analysis. *J Neurosci Res* 70:36–45.
20. Zu T, *et al.* (2004) Recovery from polyglutamine-induced neurodegeneration in conditional SCA1 transgenic mice. *J Neurosci* 24:8853–8861.
21. Garcia-Segura LM, Rodriguez JR, Torres-Aleman I (1997) Localization of the insulin-like growth factor I receptor in the cerebellum and hypothalamus of adult rats: An electron microscopic study. *J Neurocytol* 26:479–490.
22. Yamamoto A, Lucas JJ, Hen R (2000) Reversal of neuropathology and motor dysfunction in a conditional model of Huntington's disease. *Cell* 101:57–66.
23. Yue S, Serra HG, Zoghbi HY, Orr HT (2001) The spinocerebellar ataxia type 1 protein, ataxin-1, has RNA-binding activity that is inversely affected by the length of its polyglutamine tract. *Hum Mol Genet* 10:25–30.
24. Luthi-Carter R, *et al.* (2002) Polyglutamine and transcription: Gene expression changes shared by DRPLA and Huntington's disease mouse models reveal context-independent effects. *Hum Mol Genet* 11:1927–1937.
25. Gu X, *et al.* (2005) Pathological cell–cell interactions elicited by a neuropathogenic form of mutant Huntingtin contribute to cortical pathogenesis in HD mice. *Neuron* 46:433–444.
26. Garden GA, *et al.* (2002) Polyglutamine-expanded ataxin-7 promotes non-cell-autonomous Purkinje cell degeneration and displays proteolytic cleavage in ataxic transgenic mice. *J Neurosci* 22:4897–4905.
27. Custer SK, *et al.* (2006) Bergmann glia expression of polyglutamine-expanded ataxin-7 produces neurodegeneration by impairing glutamate transport. *Nat Neurosci* 9:1302–1311.
28. Garcia-Segura LM, Perez J, Pons S, Rejas MT, Torres-Aleman I (1991) Localization of insulin-like growth factor I (IGF-I)-like immunoreactivity in the developing and adult rat brain. *Brain Res* 560:167–174.
29. Ye P, D'Ercole J (1998) Insulin-like growth factor I (IGF-I) regulates IGF binding protein-5 gene expression in the brain. *Endocrinology* 139:65–71.
30. Schneider MR, Wolf E, Hoeflich A, Lahm H (2002) IGF-binding protein-5: flexible player in the IGF system and effector on its own. *J Endocrinol* 172:423–440.
31. Roschier M, *et al.* (2001) Insulin-like growth factor binding protein 5 and type-1 insulin-like growth factor receptor are differentially regulated during apoptosis in cerebellar granule cells. *J Neurochem* 76:11–20.
32. Humbert S, *et al.* (2002) The IGF-1/Akt pathway is neuroprotective in Huntington's disease and involves Huntingtin phosphorylation by Akt. *Dev Cell* 2:831–837.
33. Palazzolo I, *et al.* (2007) Akt blocks ligand binding and protects against expanded polyglutamine androgen receptor toxicity. *Hum Mol Genet* 16:1593–1603.
34. Trejo JL, Carro E, Lopez-Lopez C, Torres-Aleman I (2004) Role of serum insulin-like growth factor I in mammalian brain aging. *Growth Horm IGF Res* 14 Suppl A:S39–S43.
35. Stenvers KL, Lund PK, Gallagher M (1996) Increased expression of type 1 insulin-like growth factor receptor messenger RNA in rat hippocampal formation is associated with aging and behavioral impairment. *Neuroscience* 72:505–518.
36. Kenyon C (2005) The plasticity of aging: insights from long-lived mutants. *Cell* 120:449–460.
37. Emamian ES, *et al.* (2003) Serine 776 of ataxin-1 is critical for polyglutamine-induced disease in SCA1 transgenic mice. *Neuron* 38:375–387.
38. Chen HK, *et al.* (2003) Interaction of Akt-phosphorylated ataxin-1 with 14–3-3 mediates neurodegeneration in spinocerebellar ataxia type 1. *Cell* 113:457–468.